Eur Biophys J (2011) 40:1259–1270
DOI 10.1007/s00249-011-0713-4

ORIGINAL PAPER

EBSA
Biophysics in Europe

Zinc modulates copper coordination mode in prion protein octa-repeat subdomains

Francesco Stellato · Ann Spevacek · Olivier Proux · Velia Minicozzi · Glenn Millhauser · Silvia Morante

Received: 4 March 2011 / Revised: 29 April 2011 / Accepted: 16 May 2011 / Published online: 28 June 2011
© European Biophysical Societies' Association 2011

Abstract In this work we present and analyse XAS measurements carried out on various portions of Prion-protein tetra-octa-repeat peptides in complexes with Cu(II) ions, both in the presence and in the absence of Zn(II). Because of the ability of the XAS technique to provide detailed local structural information, we are able to demonstrate that Zn acts by directly interacting with the peptide, in this way competing with Cu for binding with histidine. This finding suggests that metal binding competition can be important in the more general context of metal homeostasis.

Keywords Prion protein · Zinc · Copper · XAS spectroscopy · Metal homeostasis

F. Stellato, A. Spevacek contributed equally to the work.

Special Issue: SIBPA Meeting 2011.

Electronic supplementary material The online version of this article (doi:10.1007/s00249-011-0713-4) contains supplementary material, which is available to authorized users.

F. Stellato · V. Minicozzi · S. Morante (✉)
Dipartimento di Fisica, Università di Roma 'Tor Vergata',
Via della Ricerca Scientifica, 1, 00133 Rome, Italy
e-mail: morante@roma2.infn.it

F. Stellato
Centre for Free-Electron Laser Science, DESY,
Notkestrasse 85, 22607 Hamburg, Germany

A. Spevacek · G. Millhauser
Department of Chemistry and Biochemistry,
University of California, Santa Cruz, CA 95064, USA

O. Proux
Observatoire des Sciences de l'Univers de Grenoble,
CNRS and Université Joseph Fourier, BP 53,
38041 Grenoble Cedex 9, France

Introduction

Transmissible spongiform encephalopathies (TSE), also known as *Prion diseases*, belong to a broad class of diseases including pathologies that can affect different species. Among these diseases we find Creutzfeldt–Jakob disease in humans, scrapie in sheep (from which the generic name for the misfolded form of the Prion protein is taken), and bovine spongiform encephalopathy (or BSE) in cattle.

There is increasing experimental evidence that in all TSEs the occurrence of an abnormal form of a protein called a Prion (shorthand for *proteinaceous infectious particle*; Prusiner 1998) protein (PrP) is of crucial importance. PrP is a membrane protein that is anchored to the membrane surface via a glycosyl phosphatidyl inositol group. It occurs in two alternative conformers: the cellular native harmless conformer, PrP^{C}, rich in α-helix, and the aberrant pathogenic conformer, PrP^{Sc} (or scrapie PrP) that has self-replicating properties and is characterized by larger β-sheet content (Gasset et al. 1993; Pan et al. 1993; Morante 2008).

The structure of the C-terminal domain of PrP^{C} has been solved by both NMR (Dominikus et al. 2005) and X-ray diffraction (Burns et al. 2002) techniques, whereas the only available structural information about PrP^{Sc} is on its secondary structure (Eghiaian et al. 2004). The unstructured N-terminal region of mammalian PrP is characterized by a highly conserved domain consisting of a variable number (from four to six depending on the species) of tandem repeats of eight amino acid residues (PHGGGWGQ) termed *octa-repeat*.

Although the structural changes characteristic of the switch between the two conformers occur in the C-terminal domain, the N-terminal region seems to have a physiological

function in subcellular trafficking (Nunziante et al. 2003). Among the different functions already tentatively attributed to PrP^C, Cu^{2+} binding is the only one that has been correlated with the physiological impairments linked to TSE (Stockel et al. 1998; Rachidi et al. 2003). The main Cu^{2+} binding site has been located within the octa-repeat region by use of several different experimental techniques (Hornshaw et al. 1995; Whittal et al. 2000; Burns et al. 2002; Qin et al. 2002; Wells et al. 2006). Other Cu^{2+} binding sites have been identified in the C-terminal globular domain (Hasnain et al. 2001; Cereghetti et al. 2001; Burns et al. 2003). Studies with PrP^C models in the form of synthetic and recombinant peptides have shown binding stoichiometries of up to one Cu^{2+} per octa-repeat group.

In previous work (Morante et al. 2004) X-ray absorption spectroscopy (XAS) was used to explore the Cu^{2+} site geometry in PrP peptides containing one, two, and four octa-repeats and in the whole recombinant form of bovine PrP (BoPrP). In that paper a model was proposed in which the Cu^{2+} coordination mode depends on the [Cu^{2+}]:[octa-repeat] concentration ratio. The model is in good agreement with the EPR results of Chattopadhyay et al. (2005), in which it is shown that Cu^{2+} can be found in three different coordination modes, called "components", whose relative abundance also depends on the [Cu^{2+}]:[octa-repeat] concentration ratio.

In particular, the geometry of the component 1 metal site is seen to be characterized by the same structure visible in the crystal (Burns et al. 2002), where the metal binding site appears to be located within the octa-repeat subsegment HGGGW. Component 2 binding is observed only in PrP structures containing two or more octa-repeat segments and EPR data have shown that there His acts as a bidentate ligand, thus giving rise to a $2N_2O$ Cu^{2+} coordination. Component 3 coordination is, instead, observed only in tri and tetra-octa-repeat structures at low Cu^{2+} concentration (<1.0 equiv.) suggesting that it only occurs if three or four sequential HGGGW segments (or in other words three or four (neutral) imidazole rings) are available.

More recently, new EPR measurements carried out by the same group (Walter et al. 2007) have shown that the presence of Zn^{2+} modulates mode of the Cu^{2+} binding to the synthetic PrP tetra-octa-repeat peptide. In particular it has been suggested that, even if Zn^{2+} is not able to completely remove Cu^{2+}, increasing the Zn^{2+} concentration can progressively change the way Cu^{2+} is bound to the tetra-octa-repeat. This modification has been interpreted in terms of variation of the relative amount of each of the three components. The question that cannot be answered by EPR experiments is by which mechanism Zn^{2+} affects Cu^{2+} binding.

In the work discussed in this paper we exploited the possibility offered by XAS spectroscopy of directly and separately looking at the structure around both Cu^{2+} and Zn^{2+} ions when they are simultaneously present in the sample, thus overcoming the intrinsic limitation of Zn^{2+} being EPR silent.

Experimental procedures

XAS experiments

XAS experiments on the Cu and Zn *K*-edges of PrP-octa-repeat samples were performed at the BM30B beamline of the European Synchrotron Radiation Facility (Grenoble, France) (Proux et al. 2005). The storage ring was operating in 16 bunches mode at 6 GeV with a ~90 mA current. The beam energy was selected using an Si(220) double-crystal monochromator with an experimental resolution close to that theoretically predicted (namely ~0.5 eV) (Proux et al. 2006). The beam spot on the sample was approximately 300 × 200 μm^2 (H × V, FWHM). Because of the low Cu^{2+} and Zn^{2+} concentrations, spectra were recorded in fluorescence mode using a 30-element solid-state Ge detector. To avoid photo-degradation and spectra evolution during XAS measurements, all the samples were cooled to 13 K (−260°C) by use of a liquid helium cryostat. To prevent Cu photo-reduction samples are moved at each scan in order for the radiation not to hit the same portion of the sample.

The energy range of Zn *K*-edge spectra is shortened by the need to avoid effects on Zn K_α fluorescence of the Cu K_β fluorescence line contribution.

XAS data analysis

For each sample the several collected spectra were first averaged and then normalized using ATHENA software (Ravel and Newville 2005). This normalization procedure is necessary to enable quantitative comparison of the X-ray absorption near edge structure (XANES) regions among different samples. ATHENA is also used to extract the $\chi(k)$ signal[1] in the extended X-ray absorption fine structure (EXAFS) region. The $\chi(k)$ data are fitted by use of the EXCURV98 package (Binsted 1998) and structural information is extracted. The theoretical expression of $\chi(k)$ is calculated by taking into account single and multiple scattering contributions (Fonda 1992). The so-called constrained refinement strategy, which consists in treating each amino acid residue as a rigid body, is used. This enables reduction of the number of free variables characterizing the

[1] For a more detailed description of how the $\chi(k)$ EXAFS signal is extracted from XAS data see the Appendix in Minicozzi et al. (2008).

Table 1 List of measured samples

Sample	$[Cu^{2+}]$ (mM)	$[Zn^{2+}]$ (mM)	Cu^{2+} bound (eq.)	Edge	C_α (%)	C_β (%)
S_1	0.16	0	0.8	Cu	0	100
S_2	0.4	0	2	Cu	80	20
S_3	0.6	0	3	Cu	100	0
S_1_Zn	0.16	0.6	0.8	Cu, Zn	55	45
S_2_Zn	0.4	0.6	2	Cu, Zn	85	15
S_3_Zn	0.6	0.6	3	Cu, Zn	100	0
B_Cu	2.0	0		Cu		
B_Zn	0	2.0		Zn		

For each sample (column 1) the concentration of Cu^{2+} in mM and equivalents (columns 2 and 4) and of Zn^{2+} in mM (column 3) is given. In column 5 the edge at which each spectrum has been collected is reported. In the last two columns we give the percentage of α and β components (see text) as obtained from Fig. 1

structural models taken into consideration in the analysis (Binsted et al. 1992).[2]

Sample preparation

Synthetic PrP octa-repeat peptides were prepared using the fluorenylmethoxycarbonyl (Fmoc) method, as previously described by Burns et al. (2002) and Aronoff-Spencer et al. (2000). The amino acid sequence of the synthetic peptide was: Ac–KKRPKPWGQ(PHGGGWGQ)$_4$–NH_2.

The initial nine amino acid residues, preceding the four consecutive octa-repeat groups present in the N-terminal of natural PrP, were inserted to increase peptide solubility. The peptide was, as usual, acetylated at the N-terminus and amidated at the C-terminus to mimic the presence of the missing portion of the natural protein. All samples were prepared by dissolving the peptide in degassed solvent containing 25 mM *N*-ethylmorpholine (NEM) buffer and 20% (*v*/*v*) glycerol at pH 7.4. The peptide concentration used for XAS samples was 0.2 mM. Cu^{2+} and Zn^{2+} were added as the salts $CuSO_4$ and $ZnCl_2$, respectively. As shown in Table 1, two classes of sample were prepared and measured: samples S_i ($i = 1, 2, 3$) prepared in the absence of Zn^{2+}, and samples S_i_Zn ($i = 1, 2, 3$), prepared in the presence of Zn^{2+}. The corresponding two buffers were also measured. In Table 1 the Cu^{2+} concentrations of the measured samples, expressed in mM (column 2) or in equivalents (column 4), are reported. In column 5 we specify the metal at the *K*-edge of which measurements had been performed. We performed 11 (i.e. 9 plus 2 for buffers) sets of measurements. In the last two columns we also list the approximate Cu^{2+} binding component percentage, extracted from EPR measurements (Walter et al. 2007). As already suggested by Walter et al. (2007), we group components 1 and 2, which for short we call component α. For uniformity of notation we then denote component 3 by β.

Results

Figure 1, where we summarize the EPR results already presented by Walter et al. (2007), clearly shows that the mode of Cu^{2+} coordination is indeed modified by the presence of Zn^{2+}. In particular it is seen that the effect of Zn^{2+} is stronger at moderate Cu^{2+} concentrations and tends to disappear at high Cu^{2+} concentration. At moderate Cu^{2+} concentrations, where Zn^{2+} is more effective, the presence of Zn^{2+} induces an increase of the α component, thus pushing the system toward Cu^{2+} binding modes in which the number of bound His units is lower.

XAS technique has the potential to (dis)prove this mechanism because, at variance with EPR, it enables direct investigation of the atomic environment of Zn^{2+}. In particular we want to discriminate between the situation in which Zn^{2+} affects the Cu^{2+} binding mode by directly binding to the peptide and the situation in which, by some more complicated and indirect mechanism, Zn^{2+} induces structural peptide modifications that in turn affect the geometry of the Cu^{2+}-binding site. With the purpose of investigating these features we acquired XAS spectra of samples with different Cu^{2+} concentrations in the absence and in the presence of Zn^{2+} at the Cu and Zn *K*-edges.

Starting with a 0.2 mM tetra-octa-repeat solution which yields a histidine concentration [His] = 0.8 mM, we prepared three samples containing Cu^{2+} at 0.16, 0.4 and 0.6 mM, corresponding to 0.8, 2 and 3 equivalents (= $[Cu^{2+}]$/[pept]), respectively (Table 1; Fig. 1).

[2] The normalization is performed in a standard way using the ATHENA software (Ravel 2008), i.e. fitting the pre-edge region with a straight line and subtracting it from the whole spectrum (Ravel and Newville 2005). The post-edge region data are then fitted with a polynomial. Finally, the jump between the pre-edge and the post-edge fits at the edge energy is calculated and the spectrum is divided by the height of the jump. We recall the standard formulae $\chi(k) = \frac{\mu(E)-\mu_0(E)}{\mu_0(E)}$ and $\hbar k = \sqrt{2m(E-E_0)}$ where $\mu_0(E)$ is the single atom absorption coefficient and E_0 is the edge energy.

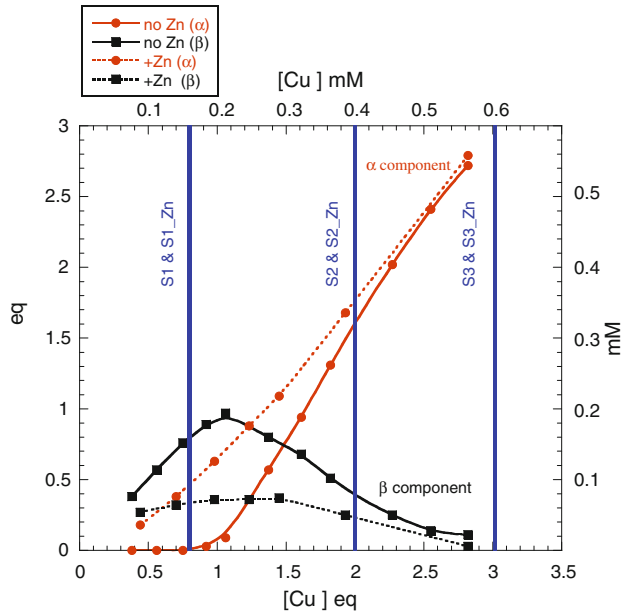

Fig. 1 Plot of α (*red*) and β (*black*) component concentrations versus Cu^{2+} concentration. *Full lines* are in the absence and *dotted lines* in the presence of Zn^{2+}. The *three blue vertical lines* are drawn to indicate the three Cu^{2+} concentrations at which XAS data were collected (Table 1). Concentrations are given both in mM (*right and top axes*) and in equivalents (*left and bottom axes*)

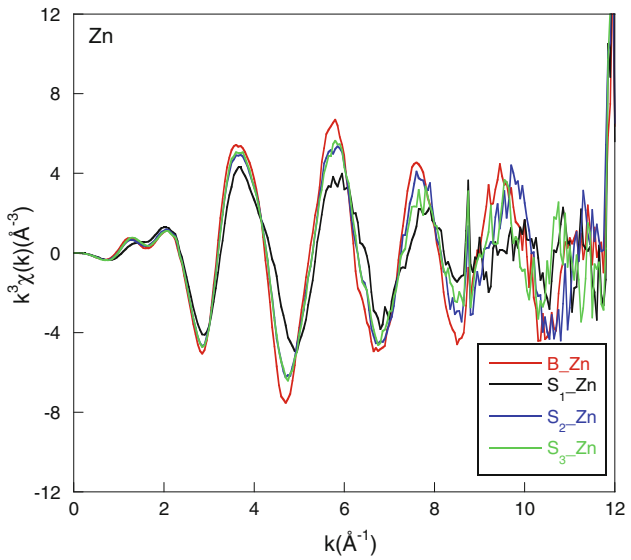

Fig. 2 Comparison among XANES spectra taken at the Cu *K*-edge of the three samples prepared at the three different Cu^{2+} concentrations of Table 1, in the absence of Zn^{2+}, namely S_1 (*black*), S_2 (*blue*), S_3 (*green*). The spectrum of the B_Cu buffer (*red*) is also shown. Here μ(E) is the normalized absorption coefficient[2]

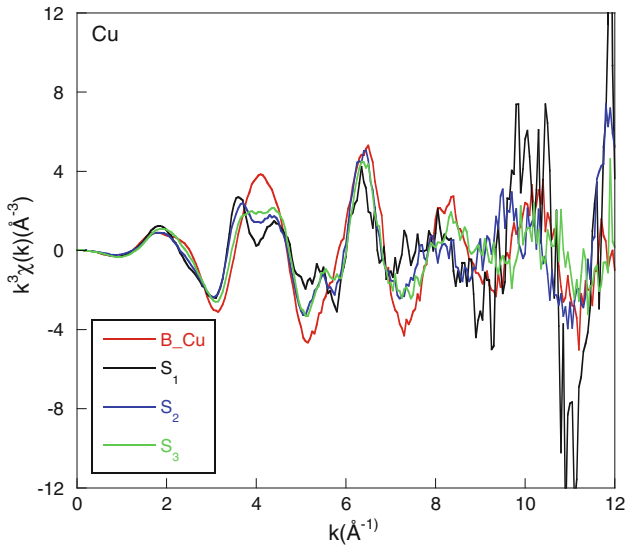

Fig. 3 The same comparison as in Fig. 2 for the EXAFS region. *Colours* are as in Fig. 2

Each solution was further subdivided into two sub-samples and 0.6 mM Zn^{2+} was added to one of these. The two reference buffer solutions were prepared as described above.

To gain an initial understanding of the structural properties of the metal (Zn^{2+} and Cu^{2+}) coordination modes, we started by examining gross similarities and differences among the many spectra we measured. For this purpose we first compared the XANES and/or EXAFS regions of the spectra qualitatively but systematically.

Qualitative XAS data analysis

From Fig. 2 it is immediately evident from the shape of the feature at the top of the sharply rising part of the spectrum (called "white line") that the spectrum of Cu^{2+} in buffer is significantly different from that of Cu^{2+} bound to the peptide at all the Cu^{2+} concentrations at which data were acquired.

In Fig. 3, the same type of comparison as in Fig. 2, but referred to the EXAFS region, is displayed. As usual, in order to partly compensate for the rapid signal decrease with increasing k, the experimental data have been multiplied by k^3. Because of the very low Cu^{2+} concentration in sample S_1, the corresponding spectrum (black line) appears to be rather noisy. Nevertheless, fixing our attention on the low-k part of the EXAFS spectrum, where noise is under control, we can observe that again the Cu-buffer (B_Cu) spectrum is markedly different from that of all the other samples, whereas the S_2 and S_3 spectra are very similar but substantially different from that of S_1. By focussing on the appearance of a double peak in the wave number region between $k \approx 3.5$ Å^{-1} and $k \approx 4.5$ Å^{-1}, which is a fingerprint feature for the presence of bound histidine residues (Ferreira et al. 2002), we can conclude that their number decreases going from S_1 to S_3, and it is obviously zero in B_Cu.

This qualitative behaviour is the same as that observed in EPR experiments (Walter et al. 2007). In fact, at low Cu^{2+} concentration (sample S_1) only the β component is

present, and its fraction decreases with increasing Cu^{2+} concentration. Indeed, the fraction of β component is already very low at 2 Cu^{2+} equivalents (sample S_2) and completely disappears at 3 Cu^{2+} equivalents (sample S_3), as seen in Fig. 1.

The same type of analysis was then performed by comparing the spectra taken at the Zn *K*-edge at the three different Cu^{2+} concentrations (samples S_i_Zn in Table 1). Now the reference spectrum is that of the Zn–buffer sample (B_Zn). Looking at the XANES region (Fig. 4), one can conclude that, at least for sample S_1_Zn, a significant amount of Zn^{2+} must be bound to the peptide, because its spectrum shows general features substantially different from that of the B_Zn sample.

The same qualitative conclusions can be drawn by studying the EXAFS part of these spectra, shown in Fig. 5. Indeed the general spectral features of S_1_Zn (which is the sample at the lowest Cu^{2+} concentration) are substantially different from those of Zn^{2+} in buffer, whereas the spectra of the samples in which the Cu^{2+} concentration is higher (S_2_Zn and S_3_Zn) are almost identical to each other and very similar to the spectrum of Zn^{2+} in buffer. In other words, the local Zn^{2+} environment in the S_1_Zn sample is significantly different from that of Zn^{2+} in solution, thus proving that at least some of the Zn^{2+} is bound to the peptide.

Finally, in order to better display the effect of Zn^{2+} on the Cu^{2+} coordination geometry, the EXAFS spectra of S_i and S_i_Zn samples are compared pair-wise in Fig. 6, focussing attention on the low-*k* region of the spectrum in which the data are statistically more accurate. The

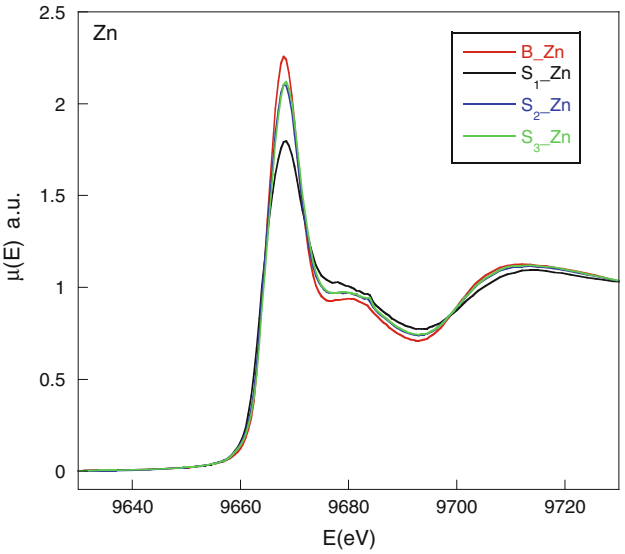

Fig. 4 Comparison among XANES spectra taken at the Zn *K*-edge of the three samples prepared at the three different Cu^{2+} concentrations of Table 1, in the presence of Zn^{2+}, namely S_1_Zn (*black*), S_2_Zn (*blue*), S_3_Zn (*green*). The spectrum of the B_Zn buffer (*red*) is also shown

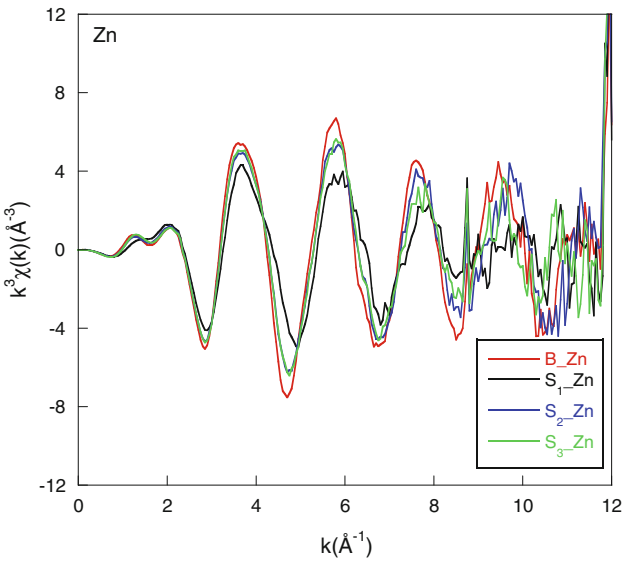

Fig. 5 Same comparison as in Fig. 4 for the EXAFS region

comparison confirms that only in sample S_1 is the mode of Cu^{2+} coordination substantially affected by the presence of Zn^{2+}.

Quantitative XAS data analysis

The qualitative analysis presented in the previous sections has led to two main conclusions:

1. the presence of Zn^{2+} does affect the mode of Cu^{2+} coordination, and
2. Zn^{2+} is able to bind to the PrP-octa-repeat domain by partially displacing Cu^{2+}.

In this section we want to make the second of these statements more quantitative and precise by trying to structurally characterize the Zn^{2+} binding site environment. This is done by fitting the EXAFS data at the Zn *K*-edge to appropriate atomic model structures.

Measurements at the Cu *K*-edge are not really useful for this discussion because the only sets of data in which the EXAFS signal-to-noise ratio is sufficiently good (i.e. those corresponding to samples S_3 and S_3_Zn) do not appear to be in any appreciable way affected by the presence of Zn^{2+}. This conclusion also follows from the EPR data of Fig. 1, in which it is clearly apparent that at this high Cu^{2+} concentration the solid lines (EPR data in the presence of Zn^{2+}) tend to coincide with the broken lines (EPR data in the absence of Zn^{2+}).[3]

[3] For completeness we provide in the supplementary material a quantitative analysis of the EXAFS spectra of samples S_3 and S_3_Zn data at the Cu K-edge. The analysis confirms that the structure of the Cu^{2+} binding site is not affected by the presence of Zn^{2+} and the fitted site geometry is highly consistent with the available crystallographic information (Chattopadhyay et al. 2005).

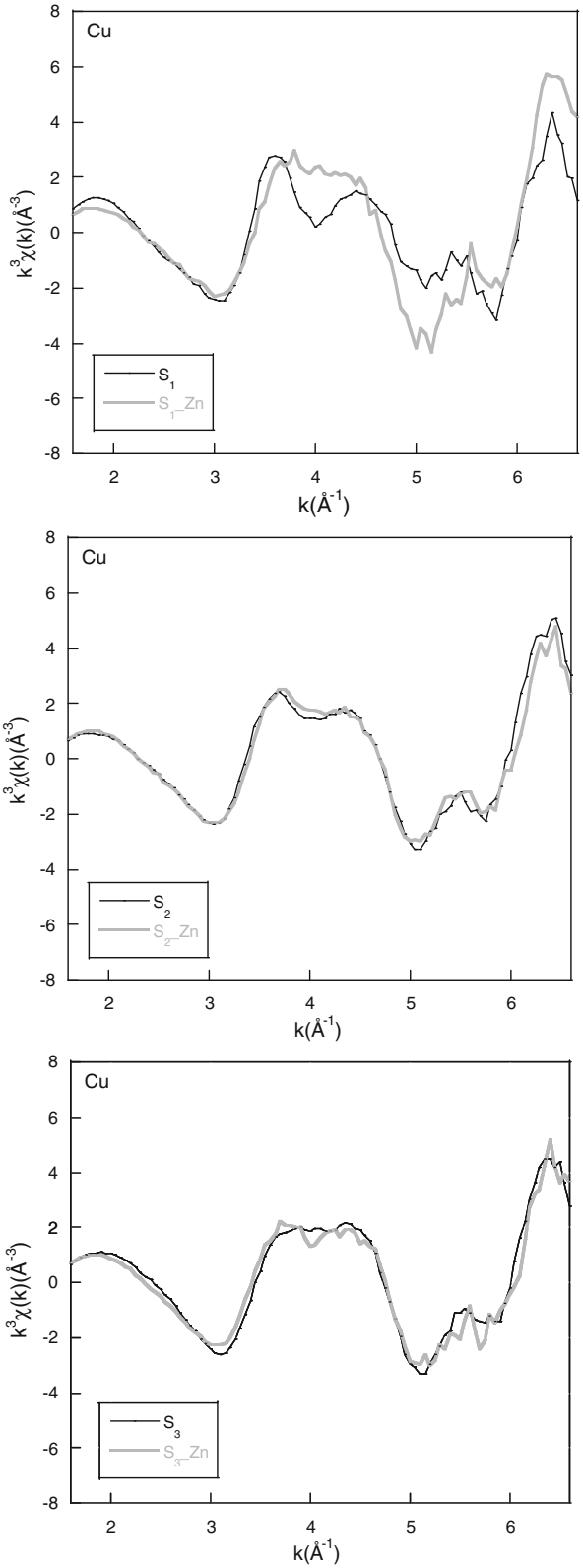

Fig. 6 Pair-wise comparison between samples in the absence, S_i, and in the presence, S_i_Zn, of Zn, in the low-k region of the EXAFS spectrum at the Cu K-edge

We shall, then, concentrate on data at the Zn K-edge, and in particular for sample S_1_Zn, for which the effect of the presence of Zn^{2+} on the Cu^{2+} coordination mode looks more pronounced (compare solid and broken curves in Fig. 1). Our objective is to extract from the XAS data the important Zn^{2+}-related structural information that is not directly available from EPR.

To proceed to quantitative analysis, we make the assumption that the Zn^{2+} can be present in our samples in two different structural configurations, one corresponding to Zn^{2+} in solution (complexed as in the buffer sample B_Zn) and the second corresponding to Zn^{2+} directly bound to the peptide. At this point, because the geometrical information that one can extract from the XAS data is the result of an average of the signals from all the structural Zn^{2+} environments, we need an estimate of the relative weight of these two Zn^{2+} coordination modes.

At a given the total His concentration, $[His]_{tot}$, the His fraction available for Zn^{2+} coordination, $[His]_{av}$, is:

$$[His]_{av} = [His]_{tot} - [His]_{Cu} \quad (1)$$

where $[His]_{Cu}$ is the His fraction that is already engaged in Cu^{2+} binding. To estimate $[His]_{Cu}$ in Eq. (1), we can exploit the EPR results of Chattopadhyay et al. (2005). EPR data show, in fact, that, in the presence of Zn^{2+} and at 0.8 Cu^{2+} equivalents (sample S_1_Zn), approximately 45% of Cu^{2+} is found in component β[4] and the remaining 55% in component α (Fig. 1), and no Cu^{2+} is found free in solution.[5] In other words, all Cu^{2+} ions are involved in some kind of peptide binding because none can be fully substituted by Zn^{2+}. This implies that the amount of His bound to Cu^{2+} can be estimated by use of the formula:

$$[His]_{Cu} = (0.45 \times 4 + 0.55 \times 1) \times 0.16\ \text{mM} = 0.38\ \text{mM}, \quad (2)$$

where the numbers 0.45 and 0.55 are the fractions of Cu^{2+} in the β and α components, respectively, and 0.16 mM is the Cu^{2+} concentration in sample S_1_Zn; the integers 4 and 1 are the numbers of His units bound to the Cu^{2+} in the β and α components, respectively.

Because, according to our assumption, the total amount of Zn^{2+} in the sample, $[Zn^{2+}]_{tot}$, is distributed between

[4] It should be said that here we have simplified the analysis by assuming that component β corresponds to a situation in which all four His units of each tetra-octa-repeat are simultaneously involved in binding the metal. For the sake of completeness, the same analysis has also been performed assuming that Cu^{2+} in component β is bound to three His units. The results obtained under this assumption do not differ from those presented here in the text and can be found in the supplementary material.

[5] The fraction of bound Cu^{2+} as a function of the Zn^{2+} concentration has been measured in Walter et al. (2007). As seen in Fig. 1 of that paper, the fraction of bound Cu^{2+} does not significantly depend on the concentration of Zn^{2+}.

Table 2 List of proposed Zn^{2+} coordination models (column 1) with n the number of Zn^{2+} bound His's (column 2)

Two-component model	n	$[Zn^{2+}]_{His}$ (in %)	$[Zn^{2+}]_{buffer}$ (in %)
M_1	1	0.42 mM (70)	0.18 mM (30)
M_2	2	0.21 mM (35)	0.39 mM (65)
M_3	3	0.14 mM (23)	0.46 mM (77)
M_4	4	0.11 mM (18)	0.49 mM (82)

Columns 3 and 4 report the Zn^{2+} concentrations (in %) bound to His units, $[Zn^{2+}]_{His}$, and free in solution, $[Zn^{2+}]_{buffer}$, respectively

Zn^{2+} bound to the peptide, $[Zn^{2+}]_{His}$, and Zn^{2+} free in solution, $[Zn^{2+}]_{buffer}$,[6] in the context of our two-component model, we obtain:

$$[Zn^{2+}]_{tot} = [Zn^{2+}]_{His} + [Zn^{2+}]_{buffer} \quad (3)$$

We also assume for simplicity that for each sample the number of His residues bound to Zn^{2+} is homogenous. We are thus led to consider four possible models, M_n, according to the number n (=1, 2, 3, and 4) of His residues bound to Zn^{2+}. With the above simplifying assumptions we obtain:

$$[Zn^{2+}]^{n}_{His} = \frac{[His]_{av}}{n} \quad (4)$$

where n is the number of His units supposed to be bound to Zn^{2+}. At this point, by use of Eq. (1), we finally obtain:

$$[His]_{av} = [His]_{tot} - [His]_{Cu} = (0.8 - 0.38)\ \text{mM} = 0.42\ \text{mM} \quad (5)$$

In Table 2 we have reported the concentrations of Zn^{2+} bound to His (column 3) together with the corresponding concentration of Zn^{2+} in the buffer (column 4) for each of the four models considered (column 1), computed using Eqs. (1)–(4).

To check the validity of this two-component model, we must first obtain reliable structural information about the atomic environment of Zn^{2+} in buffer. The best fit of the EXAFS B_Zn data is shown in Fig. 7 and is obtained by assuming Zn^{2+} is coordinated to six oxygen atoms located at a distance of 2.07 Å in octahedral geometry, as expected on the basis of, for instance, the results of D'Angelo et al. (2002a, b).

As for the S_1_Zn EXAFS spectrum, four different fits (Fig. 8) have been performed according to the number of His units assumed to be bound to Zn^{2+}. The fraction of Zn^{2+} that remains free in solution in each case can be found in Table 2.

[6] Here we make the further hypothesis that the reason why Zn^{2+} can be found free in solution it is that there are no more available His units.

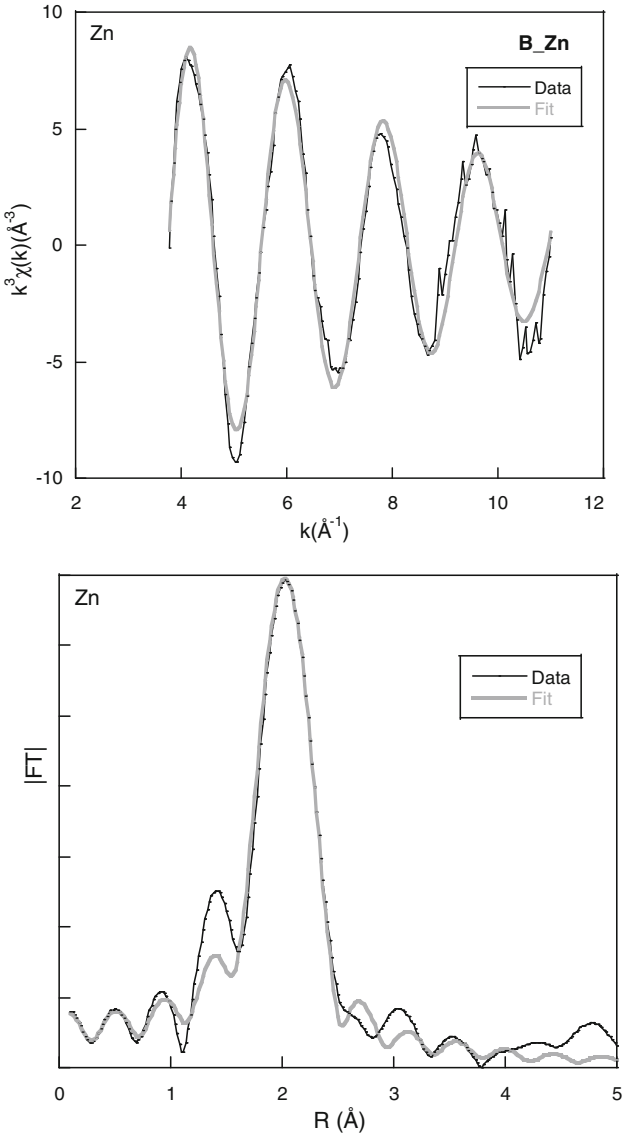

Fig. 7 Best fit of the EXAFS Zn^{2+} buffer spectrum (*upper panel*). Experimental data are in *black* and the best-fit curve is in *grey*. The amplitude of the corresponding FT spectra is shown in the *lower panel*

It is rather clear from Fig. 8 that by increasing the number of His units supposedly bound to a single Zn^{2+} ion (i.e. moving from model M_1 to model M_4) and thus correspondingly increasing the fraction of Zn^{2+} in solution (Table 2), the quality of the fit (quantified in terms of the standard quality factor, R[7]) significantly deteriorates.[8]

[7] The quality factor R is computed by use of the formula: $R = \sum_{i=1}^{P} \frac{1}{w_i} \left| \chi^{exp}(k_i) - \chi^{fit}(k_i) \right|$ where P is the number of experimental points and $w_i = \frac{1}{k_i^n} \sum_{j=1}^{P} k_j^n |\chi^{exp}(k_j)|$ in which n is an integer which is normally taken to lie between 0 and 3 (here we took $n = 3$).

[8] In all the fits only the distance and relative position of the nearest neighbouring atoms in the His-bound Zn^{2+} environment are taken as free variables.

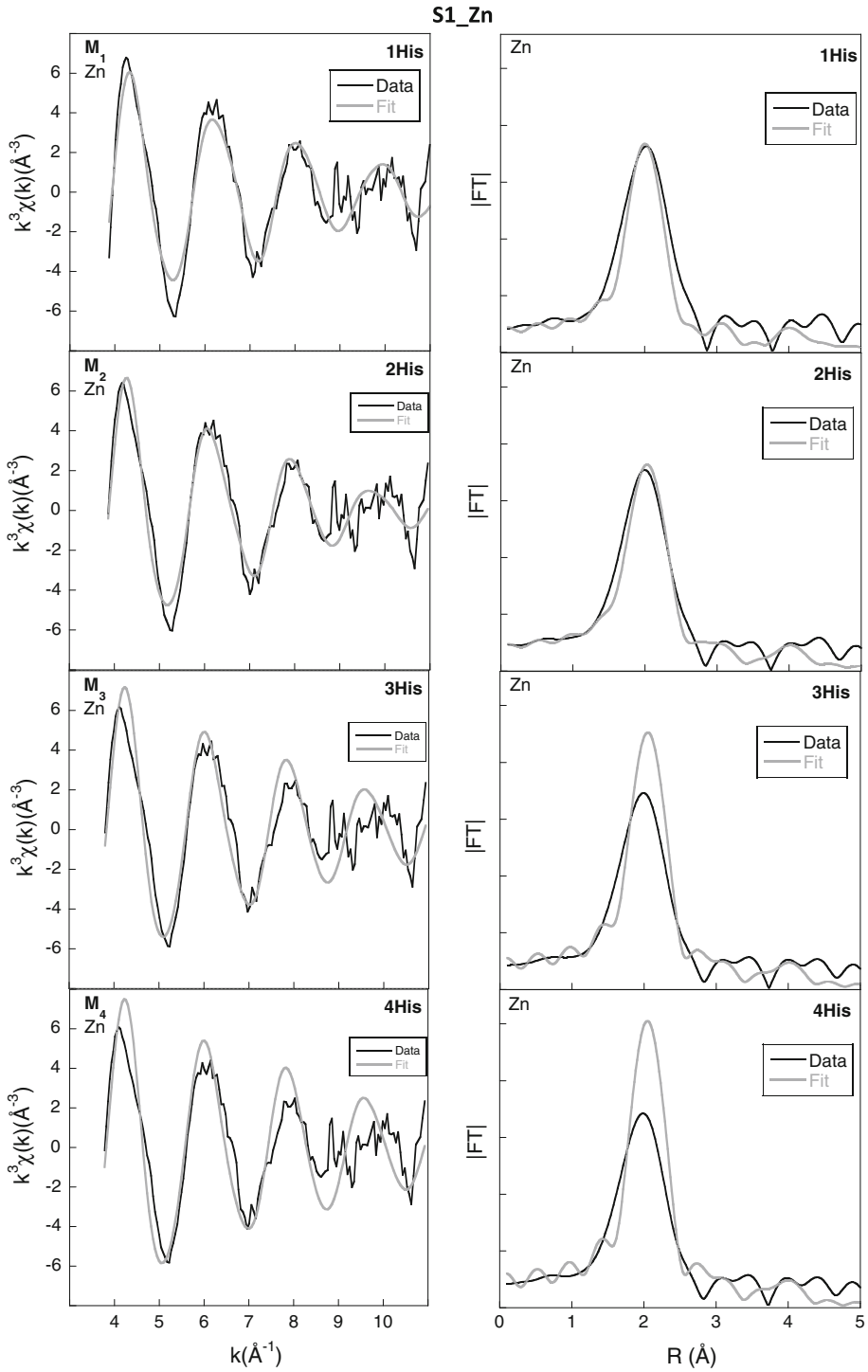

Fig. 8 Comparison between experimental XAS spectra of sample S_1_Zn at the Zn *K*-edge (*black*) and the simulated spectra (*grey*) corresponding to the four models of Table 2. EXAFS data are shown in the *left column*. The amplitudes of the corresponding FT spectra are displayed in the *right column*

In particular, R seems to be unacceptably high for models M_3 and M_4 (49 and 60%, respectively). In contrast, it decreases to rather good values, 34 and 35%, for models M_1 and M_2.

The net outcome of the analysis is that there are qualitative and quantitative reasons to discard models M_3 and M_4 as unphysical, and, although we do not have enough "resolution" to choose between models M_1 and M_2, they seem to yield a quite accurate description of the Zn^{2+} structural environment.[9]

[9] Incidentally, we have also tried to leave the Zn^{2+} fraction in buffer as a free variable in the fit to the S_1_Zn XAS spectra (data not shown). Values in good agreement with the numbers in the second column of Table 2 are obtained when the structural models M_1 and/or M_2 are assumed. Completely unrealistic values are instead selected by the fit with models M_3 and M_4.

We end by noting that in the Fourier transform (FT) of the simulated spectra the peak at approximately 3 Å (which is a fingerprint of the presence of histidine and is expected to become increasingly intense with the number of bound histidines (Strange et al. 1990)) is not visible in our case, because, as we explained above, in the situation in which more histidines are bound to Zn^{2+}, more Zn^{2+} is found in solution (Table 2). Indeed, because the simulated XAS spectrum is the result of the sum of the features coming from all possible Zn^{2+} coordination modes, the histidine peak is either too small (when only one histidine is bound) or obscured by the superimposed contribution coming from Zn^{2+} in buffer (when a larger number of histidines is bound).

Fourier transform and BVS analysis

Further information about the structure of the Zn^{2+} binding site, confirming our previous results, can be extracted by using the FT of the XAS spectra obtained from sample S_i_Zn ($i = 1, 2, 3$) to set up a bond valence sum (BVS) analysis (Brown and Altermatt 1985).

Assuming the validity of the two-component model described above, we expect the location, $\langle r_i^{\mathrm{FT}} \rangle$, of the main peak in the |FT| (i.e. the mean distance of the first shell atoms from the metal), to be given by the formula:

$$\langle r_i^{\mathrm{FT}} \rangle = \frac{x_{in} \times 6 \times \langle r_{\mathrm{buffer}} \rangle + (1 - x_{in}) \times 4 \times \langle r_{in} \rangle}{x_{in} \times 6 + (1 - x_{in}) \times 4} \tag{6}$$

in which the ratio:

$$x_{in} = \frac{[\mathrm{Zn}^{2+}]^{in}_{\mathrm{buffer}}}{[\mathrm{Zn}^{2+}]_{\mathrm{total}}} \tag{7}$$

represents the fraction of Zn^{2+} free in solution in the three S_i_Zn ($i = 1, 2, 3$) samples expected for the four models M_n ($n = 1, 2, 3, 4$). The quantity $[Zn^{2+}]^{in}_{\mathrm{buffer}}$ is computed by use of Eqs. (3) and (4) and hence depends on the sample and the model. In Eq. (6) $\langle r_{\mathrm{buffer}} \rangle$ is the Zn^{2+} first shell mean distance of the (x_{in} fraction of) Zn^{2+} that is free in solution. From the fit to the XAS data we find $\langle r_{\mathrm{buffer}} \rangle = 2.07$. Finally $\langle r_{in} \rangle$ is the Zn^{2+} first shell mean distance of the remaining ($1 - x_{in}$) Zn^{2+} fraction bound to the peptide and represents the unknown quantity we ought to determine in the different situations under study. The coordination number is taken to be 6 for Zn^{2+} in solution and 4 for Zn^{2+} bound to the peptide.

In Table 3 the quantities appearing in Eq. (6) for all the samples (column 1), $i = 1, 2, 3$, and all the models (column 2), $n = 1, 2, 3, 4$, are reported. The first shell mean distance, $\langle r_i^{\mathrm{FT}} \rangle$ (column 3), is obtained by first shell Fourier filtered data fitting in which four oxygen Zn^{2+} coordination is assumed. The values of $\langle r_{in} \rangle$, obtained solving Eq. (6), are reported in column 5.

Table 3 Summary of the results from analysis of the four proposed Zn^{2+} coordination models, M_n

Sample	Model	$\langle r_i \rangle$ (Å)	x_{in}	$\langle r_{in} \rangle$ (Å)	$(\mathrm{BVS})_{in}$
S_1_Zn	M_1	2.026 ± 0.009	0.30	1.99 ± 0.02	1.88 ± 0.08
	M_2		0.65	1.89 ± 0.03	2.5 ± 0.3
	M_3		0.77	1.78 ± 0.05	3.3 ± 0.5
	M_4		0.82	1.67 ± 0.07	4.6 ± 0.9
S_2_Zn	M_1	2.051 ± 0.007	0.58	2.00 ± 0.02	1.8 ± 0.1
	M_2		0.79	1.92 ± 0.04	2.3 ± 0.4
	M_3		0.86	1.83 ± 0.07	2.9 ± 0.5
	M_4		0.90	1.7 ± 0.1	4 ± 1
S_3_Zn	M_1	2.075 ± 0.007	0.67	2.08 ± 0.03	1.5 ± 0.1
	M_2		0.83	2.08 ± 0.05	1.5 ± 0.2
	M_3		0.89	2.08 ± 0.09	1.5 ± 0.4
	M_4		0.92	2.1 ± 0.1	1.5 ± 0.5
Buffer		2.075 ± 0.005			2.2 ± 0.2

Column 1 shows the measured samples, column 2 the proposed model, column 3 the fraction of Zn^{2+} in buffer (from Eq. (7)), column 4 the mean first shell distance (computed from Eq. (6)), column 5 the (BVS) values computed from Eq. (9)

With this information available a possible means of choosing among the different metal coordination modes is computation of the so-called bond valence sum (BVS) (Brown and Altermatt 1985). The value of BVS is, in fact, expected to be approximately the formal oxidation number of the metal ion, i.e. 2 in our case. (BVS) is computed by use of the formula:

$$(\mathrm{BVS}) = \sum_{\ell} \exp \frac{r_\ell^{(0)} - \langle r_\ell \rangle}{B_\ell}, \tag{8}$$

where the sum over ℓ extends over the contributions from all the metal ligands. The quantities $r_\ell^{(0)}$ and B_ℓ are phenomenological variables depending on the nature of metal and ligands, and can be found in Thorp (1992). In our case Zn^{2+} is bound to four ligands, all at the same distance, which can be either O or N, according to the model we consider (column 2 of Table 3). Because $r^{(0)}$ and B for O and N are very similar, with $r^{(0)}_{\mathrm{Zn}-N} = 1.72$ Å (Brown 2010), $r^{(0)}_{\mathrm{Zn}-O} = 1.70$ Å, and $B_{\mathrm{Zn}-O} \approx B_{\mathrm{Zn}-N}$ (34), Eq. (8) can be usefully simplified to the form:

$$(\mathrm{BVS})_{in} = 4 \times \exp \frac{\bar{r}^{(0)} - \langle r_{in} \rangle}{B} \tag{9}$$

with $\bar{r}^{(0)}$ the average value between $r^{(0)}_{\mathrm{Zn}-N}$ and $r^{(0)}_{\mathrm{Zn}-O}$. Indices i and n (with the meaning specified above) which have been appended to BVS as the actual Zn–ligand distances, $\langle r_{in} \rangle$, depend both on the model and the sample.

The BVS values computed according to Eq. (9) are given in the last column of Table 3.

Looking at the whole set of numbers reported in Table 3, the first striking observation is that in sample S_3_Zn, the mean distance obtained from the |FT| data (column 3) is equal, within experimental error, to the first shell distance of Zn^{2+} in buffer (last row). This equality leads in turn to values of $\langle r_{3n} \rangle$ that are perfectly consistent with the first shell distance of Zn^{2+} in buffer. We then conclude that in sample S_3_Zn, Zn^{2+} is free in solution, and Eq. (6) loses its meaning, because in this case Zn^{2+} is expected to be coordinated by six ligands.

Information contained in BVS can be used to identify the range of "acceptable" values for the fraction, x_{in}, of Zn^{2+} free in solution in each sample. For this purpose we exploit Eq. (9) to obtain the $\langle r_{in} \rangle$ values corresponding to an acceptable BVS range of values for the Zn^{2+} oxidation number. A 10% error is normally attributed to a BVS calculation, thus leading to the acceptable interval ($BVS_{min} = 1.8$, $BVS_{max} = 2.2$). Inverting Eq. (9) leads to $r_{max} = 2.01$ Å and $r_{min} = 1.93$ Å. In Fig. 9 $\langle r_{in} \rangle$ is plotted against x_{in}, with the two horizontal lines drawn in correspondence to r_{max} and r_{min}.

Continuous lines are obtained from Eq. (6), whereas full dots indicate the x_{in} values corresponding to the four M_n models. The vertical lines identify the region of "acceptable" x_{in} values for sample S_1_Zn (red) and S_2_Zn (blue) according to our criteria. In particular x_{in} is found to lie between 0.18 and 0.56 for sample S_1_Zn and between 0.54 and 0.78 for sample S_2_Zn. These findings are in agreement with the values (0.30 and 0.58, respectively) one obtains for x_{in} by assuming that in both samples Zn is bound as in model M_1 (Table 3). It should be noted, however, that for sample S_2_Zn, the binding mode suggested in model M_2 cannot be completely excluded.[10]

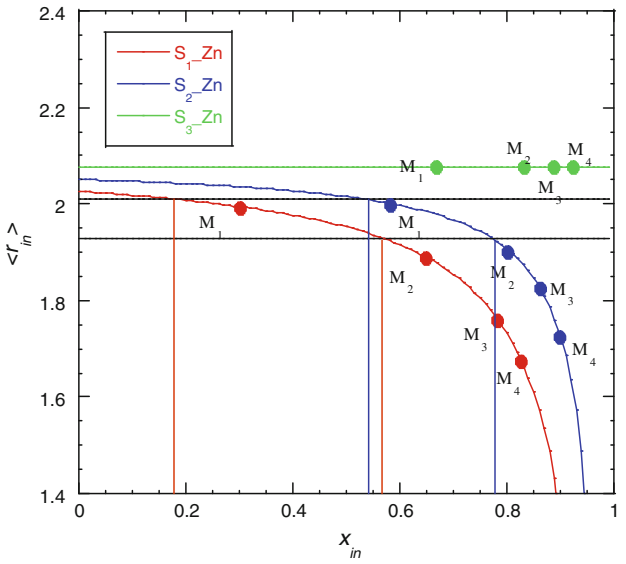

Fig. 9 The *three curves* are obtained by plotting $\langle r_{in} \rangle$ against x_{in} as computed from Eq. (6) for S_1_Zn (*red*), S_2_Zn (*blue*), and S_3_Zn (*green*). *Full dots* correspond to the values given in Table 3. *Horizontal black lines* are drawn in correspondence to the r_{max} and r_{min} values computed from Eq. (9). *Vertical, red and blue lines* are drawn from the point where each curve intersects the *horizontal black lines*, thus limiting the interval of acceptable x_{in} values

With regard to sample S_3_Zn (green line), the BVS values are not informative, because, as we said above, the hypothesis of a fourfold coordination in Eq. (9) cannot be true if all Zn^{2+} is supposed to be in solution. On the other hand, assuming that in the buffer Zn is coordinated to six ligands, the very good value $BVS_{buffer} = 2.2 \pm 0.2$ is obtained (last line of Table 3).

Discussion

In this paper we have shown that XAS measurements can be used to clarify the mechanism of Cu^{2+} affinity modulation induced by Zn^{2+} that was left open in Walter et al. (2007). We have found that Zn^{2+} modifies the Cu^{2+} coordination mode by directly interacting with the PrP peptide. This conclusion can be directly inferred from the fact that the XAS spectrum of sample S_1_Zn is definitely different from that of Zn^{2+} in buffer (Figs. 4 and 5).

The most natural hypothesis of the way Zn^{2+} interacts with the peptide is to assume that it directly binds His units. In fact, EPR results have shown that the presence of Zn^{2+} promotes the partial switch of Cu^{2+} coordination mode from component β, in which the Cu^{2+} is bound to four His units, to component α, in which only one His is bound to Cu^{2+} (see Walter et al. 2007 and Fig. 1) suggesting that Zn^{2+} competes for His binding.

Under the assumption that this picture is correct, one can compute the number of His units involved in Zn^{2+} binding. Careful analysis based on XAS data and (BVS) calculation leads to the conclusion that the number of Zn^{2+} bound His units is most probably one and certainly no larger than two (Fig. 9 and Table 3).

The analysis presented in the paper confirms the important result of Walter et al. (2007) according to which Cu^{2+} is never completely removed by Zn^{2+}. This finding suggests that the Cu–His binding strength depends on the number of His units already bound to Cu^{2+}. Results in this direction are obtained by the numerical computation carried out by Guerrieri et al. (2009), in which the effect of

[10] In the supplementary material the same plot as in Fig. 9 is drawn by also taking into account the errors in the $\langle r_{in} \rangle$ determination. In this way both M_1 and M_2 models yield numbers for $\langle r_{in} \rangle$ that fall within the range of the acceptable BVS values as defined in the text.

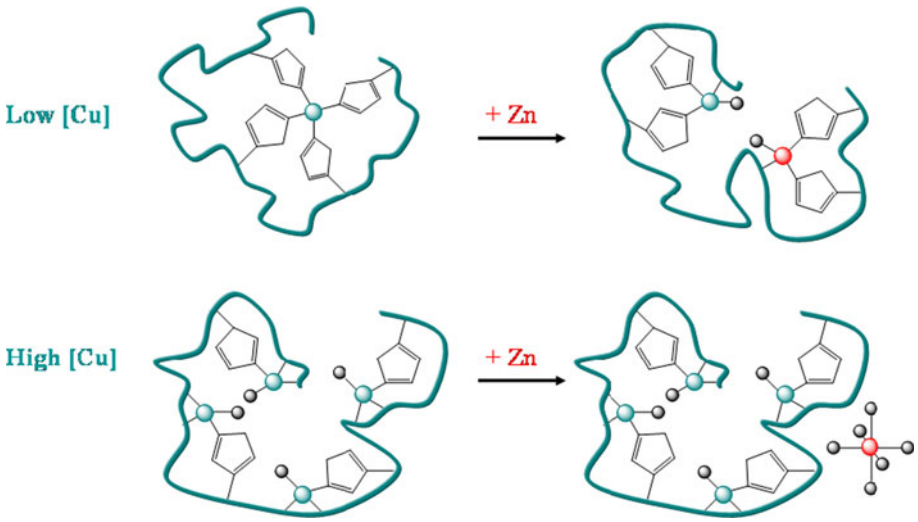

Fig. 10 Sketch of Zn^{2+} action at low (*upper reaction*) and high (*lower reaction*) Cu^{2+} concentration. The tetra-octa-repeat is drawn as a *blue string*. His units are shown explicitly. *Green dot* is Cu^{2+}, *red dot* is Zn^{2+}, and *grey dots* are water oxygens

Gly deprotonation is shown to be crucial in determining the metal coordination mode.

In Fig. 10 we show a sketch of the structural modifications induced by adding Zn. In the first reaction (upper line) that occurs at low Cu^{2+} concentration in which only the β component is present, Zn^{2+} binds one or two His units, displacing Cu^{2+}. The second reaction (lower line) shows that when Cu^{2+} concentration is sufficiently high to have only the α component, Zn^{2+} is no longer able to remove Cu^{2+} and no longer interacts with the peptide, thus having only very limited effect on the Cu^{2+} coordination mode.

We close with a comment concerning the interesting result reported by Walter et al. (2007), in which DEPC modification followed by mass spectroscopy was used to measure Zn^{2+} affinity for PrP peptides, spanning both the non-octa-repeat Cu^{2+} binding sites, PrP(90–114), and the octa-repeat region, PrP(60–91). Experiments have shown that, in the absence of Cu^{2+}, Zn^{2+} only binds to the octa-repeat region with all four octa-repeats engaged in a stable Zn^{2+} to four-His units bonded configuration. The lack of Zn^{2+} binding to PrP peptides with fewer than four octa-repeats emerging in DEPC modification experiments may seem to contradict the result found here according to which, in the presence of Cu^{2+}, a Zn^{2+} ion can be found to bind one His by partially displacing Cu^{2+}. To reconcile simultaneous Cu^{2+} and Zn^{2+} uptake, Walter et al. (2007) proposed the coexistence in solution of two metal-bound PrP species: one with a single Zn^{2+} coordinated by four His residues and another in which each of the four available His units is bound to a Cu^{2+} ion. This picture, however, does not clarify the reason for the effect of Zn on the Cu coordination mode.

The results in this paper provide a rather different and simpler picture in which a single octa-repeat domain takes up both Cu^{2+} and Zn^{2+}. Moreover, our findings suggest that Cu^{2+} may introduce a kink or local conformation that assists Zn^{2+} binding in a somewhat unusual 2-His coordination mode, as shown in Fig. 10. This kind of binding leads to a mechanism of cross-regulation between Cu^{2+} and Zn^{2+} that is worth further investigation in other biological systems (for example the Aβ-peptides involved in Alzheimer's disease). This mechanism may, in fact, suggest the existence of an additional general strategy for fine regulation of metal binding to avoid cell damage.

Acknowledgments We are very grateful to G.C. Rossi for useful discussions and for reading the manuscript. Partial financial support from PRIN08 is acknowledged. We thank the anonymous referees for their useful suggestions.

References

Aronoff-Spencer E, Burns CS, Avdievich NI, Gerfen GJ, Peisach J, Antholine WE, Ball HL, Cohen FE, Prusiner SB, Millhauser GL (2000) Identification of the Cu^{2+} binding sites in the N-terminal domain of the prion protein by EPR and CD spectroscopy. Biochemistry 39:13760–13771

Binsted N (1998) EXCURV98. CCLRC Daresbury Laboratory, Warrington, Cheshire, UK

Binsted N, Strange RW, Hasnain SS (1992) Constrained and restrained refinement in EXAFS data analysis with curved wave theory. Biochemistry 31:12117–12125

Brown ID (2010) Private communication (see also www.mrl.ucsb.edu/~seshadri/2009_218/bvparm2006.pdf)

Brown ID, Altermatt D (1985) Bond-valence parameters obtained from a systematic analysis of the inorganic crystal structure database. Acta Cryst B4:244–247

Burns CS, Aronoff-Spencer E, Dunham CM, Lario P, Avdievich NI, Antholine WE, Olmstead MM, Vrielink A, Gerfen GJ, Peisach J, Scott WG, Millhauser GL (2002) Molecular features of the copper binding sites in the octarepeat domain of the prion protein. Biochemistry 41:3991–4001

Burns CS, Aronoff-Spencer E, Legname G, Prusiner SB, Antholine WE, Gerfen GJ, Peisach G, Millhauser GL (2003) Copper

coordination in the full-length, recombinant prion protein. Biochemistry 42:6794–6803
Cereghetti GM, Schweiger A, Glockshuber R, Van Doorslaer S (2001) Electron paramagnetic resonance evidence for binding of Cu2+ to the C-terminal domain of the murine prion protein. Biophys J 81:516–525
Chattopadhyay M, Walter ED, Newell DJ, Jackson PJ, Aronoff-Spencer E, Peisach J, Gerfen GJ, Bennett B, Antholine WE, Millhauser GL (2005) The octarepeat domain of the prion protein binds Cu(II) with three distinct coordination modes at pH 7.4. J Am Chem Soc 127(36):12647–12656
D'Angelo P, Benfatto M, Della Longa S, Pavel NV (2002a) Combined XANES and EXAFS analysis of Co^{2+}, Ni^{2+}, and Zn^{2+} aqueous solutions. Phys Rev B 66:064209
D'Angelo P, Barone V, Chillemi G, Sanna N, Meyer-Klaucke W, Pavel NV (2002b) Hydrogen and higher shell contributions in Zn^{2+}, Ni^{2+}, and Co^{2+} aqueous solutions: an X-ray absorption fine structure and molecular dynamics study. J Am Chem Soc 124:1958–1967
Dominikus AL, Schorn C, Nivon LG, Esteve-Moya V, Christen B, Calzolai L, von Schroetter C, Fiorito F, Herrmann T, Güntert P, Wüthrich K (2005) Prion protein NMR structures of cats, dogs, pigs, and sheep. Proc Natl Acad Sci USA 102:640–645
Eghiaian F, Grosclaude J, Lesceu S, Debey P, Doublet B, Tréguer E, Rezaei H, Knossow M (2004) Insight into the PrPC→PrP(SC) conversion from the structures of antibody-bound ovine prion scrapie-susceptibility variants. Proc Natl Acad Sci USA 101: 10254–10259
Ferreira GC, Franco R, Mangravita A, George GN (2002) Unraveling the substrate-metal binding site of ferrochelatase: an X-ray absorption spectroscopic study. Biochemistry 41:4809–4818
Fonda L (1992) Multiple-scattering theory of X-ray absorption: a review. J Phys Condens Matter 4:8269–8302
Gasset M, Baldwin MA, Fletterick RJ, Prusiner SB (1993) Perturbation of the secondary structure of the scrapie prion protein under conditions that alter infectivity. Proc Natl Acad Sci USA 90:1–5
Guerrieri F, Minicozzi V, Morante S, Rossi GC, Furlan S, La Penna G (2009) Modeling the interplay of glycine protonation and multiple histidine binding of copper in the prion protein octarepeat sub-domains. J Biol Inorg Chem 14:361–374
Hasnain SS, Murphy LM, Strange RW, Grossmann JG, Clarke AR, Jackson GD, Collinge J (2001) XAFS Study of the High-affinity Copper-binding Site of Human PrP91–231 and its low-resolution structure in solution. J Mol Biol 311:467–473
Hornshaw MP, McDermott JR, Candy JM, Lakey JH (1995) Copper binding to the N-terminal tandem repeat region of mammalian and avian prion protein: structural studies using synthetic peptides. Biochem Biophys Res Commun 214:993–999
Minicozzi V, Stellato F, Comai M, Dalla Serra M, Potrich C, Meyer-Klaucke W, Morante S (2008) Identifying the minimal Cu and Zn binding site sequence in amyloid beta peptides. J Biol Chem 283:10784–10792
Morante S (2008) Metal ions and protein aggregation: the case of prion protein and β-amyloids (invited review). In: Bulone D, San Biagio PL (eds) Biophysical inquiry into protein aggregation and amyloid diseases, research signpost edition. Transworld Research Network, Kerala, pp 53–110
Morante S, González-Iglesias R, Potrich C, Meneghini C, Meyer-Klaucke W, Menestrina G, Gasset M (2004) Inter- and intra-octarepeat Cu(II) site geometries in the prion protein. Implication in Cu(II) binding cooperativity and Cu(II)-mediated assemblies. J Biol Chem 279:11753–11759
Nunziante M, Gilch S, Schatzl HM (2003) Essential rôle of the prion protein N terminus in subcellular trafficking and half-life of cellular prion protein. J Biol Chem 278:3726–3734
Pan KM, Baldwin M, Nguyen J, Gasset M, Serban A, Groth D, Mehlhorn I, Huang Z, Fletterick RJ, Cohen FE, Prusiner SB (1993) Conversion of α-Helices β-sheets features in the formation of the scrapie prion proteins. Proc Natl Acad Sci USA 90:10962–10966
Proux O, Biquard X, Lahera E, Menthonnex J–J, Prat A, Ulrich O, Soldo Y, Trévisson P, Kapoujvan G, Perroux G, Taunier P, Grand D, Jeantet P, Deleglise M, Roux J-P, Hazemann J-L (2005) FAME: A new beamline for X-ray absorption investigations of very-diluted systems of environmental, material and biological interests. Phys Scripta 115:970–973
Proux O, Nassif V, Prat A, Ulrich O, Lahera E, Biquard X, Menthonnex J–J, Hazemann J-L (2006) Feedback system of a liquid nitrogen cooled double-crystal monochromator: design and performances. J Synchrotron Radiat 13:59–68
Prusiner SB (1998) Prions. Proc Natl Acad Sci USA 95:13363–13383
Qin K, Yang Y, Mastrangelo P, Westaway D (2002) Mapping Cu(II) binding sites in prion proteins by diethyl pyrocarbonate modification and matrix-assisted laser desorption ionization-time of flight (MALDI-TOF) mass spectrometric footprinting. J Biol Chem 277:1981–1990
Rachidi W, Mange A, Senator A, Guiraud P, Riondel J, Benboubetra M, Favier A, Lehmann S (2003) Prion infection impairs copper binding of cultured cells. J Biol Chem 278:14595–14598
Ravel B (2008) ATHENA user's guide. http://cars9.uchicago.edu/ravel/software/exafs/
Ravel B, Newville M (2005) ATHENA, ARTEMIS, HEPHAESTUS: data analysis for X-ray absorption spectroscopy using IFEFFIT. J Synchrotron Rad 12:537–541
Stockel J, Safar J, Wallace AC, Cohen FE, Prusiner SB (1998) Prion protein selectively binds copper(II) ions. Biochemistry 37:7185–7193
Strange RW, Alagna L, Durham P, Hasnain SS (1990) An understanding of the x-ray absorption near-edge structure of copper(II) imidazole complexes. J Am Chem Soc 112:4265–4268
Thorp HH (1992) Bond valence sum analysis of metal-ligand bond lengths in metalloenzymes and model complexes. Inorg Chem 31:1585–1588
Walter ED, Stevens DJ, Visconte MP, Millhauser GL (2007) The prion protein is a combined zinc and copper binding protein: Zn^{2+} alters the distribution of Cu^{2+} coordination modes. J Am Chem Soc 129:15440–15441
Wells MA, Jelinska C, Hosszu LLP, Craven CJ, Clarke AR, Collinge J, Waltho JP, Jackson GS (2006) Multiple forms of copper (II) co-ordination occur throughout the disordered N-terminal region of the prion protein at pH 7.4. Biochem J 400:501–510
Whittal RM, Ball HL, Cohen FE, Burlingame AL, Prusiner SB, Baldwin MA (2000) Copper binding to octarepeat peptides of the prion protein monitored by mass spectrometry. Protein Sci 9:332–343